Structure and Charge Density of a C_{60}-Fullerene Derivative Based on a High Resolution Synchrotron Diffraction Experiment at 100 K

Armin Wagner, Ralf Flaig, Dieter Zobel, Birger Dittrich, Petra Bombicz, Marianna Strümpel, and Peter Luger*

Institute for Chemistry/Crystallography, Free University of Berlin, Takustrasse 6, 14195 Berlin, Germany

Tibor Koritsanszky*

Chemistry Department, State University of New York at Buffalo, Buffalo, New York 14260-3000

Hans-Georg Krane

Institute for Mineralogy and Petrology, University of Bonn, Poppelsdorfer Schloss, 53115 Bonn, Germany

Received: December 13, 2001; In Final Form: April 24, 2002

The experimental charge density of a highly substituted fullerene derivative, the T_h-symmetrical dodekakis-(ethoxycarbonyl)-C_{60}-fullerene cocrystallized with difluorobenzene, $C_{102}H_{60}O_{24}\cdot 2C_6H_4F_2$, was determined, on the basis of a high-resolution synchrotron/CCD data set of more than 350 000 reflections. A full topological analysis, using Bader's AIM theory, was performed. Experimental bond critical point (BCP) properties, obtained by three multipole models, were compared to each other and to those derived by theoretical methods from HF/6-31G** and from B3LYP/6-31G** calculations. $\rho(\mathbf{r}_{BCP})$ vs bond distance relationships were investigated for the different experimental and theoretical models. Based on linear fits obtained for experimental model densities, $\rho(\mathbf{r}_{BCP})$ values of further C−C bonds can be predicted. Due to substitution, this C_{60} derivative has six chemically different C−C bonds. A statistical analysis of the BCP properties for these bonds was carried out to explore the reproducibility of different topological descriptors.

Introduction

Charge density studies on fullerenes are still challenging tasks, although the application of high-intensity synchrotron radiation, area detectors, and stable cooling devices have made it possible to collect large X-ray data sets of high resolution and accuracy within a short period of time.[1−4] These revolutionary technical advances allow us to study the crystal charge density, $\rho(\mathbf{r})$, of small molecules almost routinely. Comparative studies on an entire class of chemically related compounds became also feasible[5] and considerable effort is being made to extend the method to larger systems.[6−8] Parallel to the experimental progress, new density-based quantum chemical methods have gained widespread applications, not only in predicting molecular properties (density functional theory, DFT)[9] but also in interpreting these in terms of basic concepts of chemistry (theory of Atoms in Molecules, AIM).[10] The topological theory has provided a powerful tool for the analysis of X-ray charge densities and led to qualitative and quantitative chemical information, necessary for understanding the electronic structure of molecules and solids.[11]

The vast majority of experimental studies, aiming at the extraction of bond topological properties from X-ray data, compare their results with those obtained by quantum chemical calculations.[11] Such a comparison is not straightforward due to the fundamentally different nature of the two methods. The topology of theoretical densities is influenced by the level of approximation and the basis set applied, while experimental densities depend on the precision and resolution of the data, the adequacy of the model, and the refinement strategy followed during the data interpretation. Commonly used multipole models[12] can lead to experimental $\rho(\mathbf{r}_{BCP})$ values (the density at the bond critical point $\mathbf{r}_{BCP}$, where $\nabla\rho(\mathbf{r}_{BCP}) = 0$) in exceptionally good agreement with those predicted by ab initio methods, especially for C−C bonds.[13] However, considerable differences have been obtained for $\nabla^2\rho(\mathbf{r}_{BCP})$ (the Laplacian at the BCP), though to a lesser extent for nonpolar than for polar bonds.[14] It became evident that the source of the latter disagreement is the bond curvature (the positive eigenvalue of the Hessian formed from the second derivatives of $\rho(\mathbf{r})$ at $\mathbf{r}_{BCP}$), whose experimental values often lack correlation with their theoretical counterparts.[15] A recent model study emphasizes the limitation of the multipole formalism in reproducing fine details of the density along a bond path.[16] The inadequacy lies in the atomic deformation radial functions, which with fixed exponents (energy-optimized for the isolated atom at the single-ζ level)[17] do not provide the necessary flexibility. The refinement of the orbital exponents against X-ray data (κ' refinement, where κ' scales the exponent) is often troublesome and avoided. To overcome this difficulty, a κ'-restricted multipole model (KRMM) was proposed, in which κ' parameters calibrated to ab initio densities were used in the interpretation of X-ray data.[18] A small library of radial screening factors for C, O, N, and H atoms, in their most common chemical environment, has recently been published.[19]

The correlation of BCP properties with the bond length (or with the bond path length, the path of maximum density interconnecting two interacting atoms) has been extensively studied by both theoretical[20] and experimental methods.[21] Simple relationships could be established, especially for C−C bonds formed between atoms in their typical hybridizations. An

10.1021/jp0145199 CCC: $22.00
Published on Web 06/21/2002

SCHEME 1: Formula Scheme of the Title Compound $C_{102}H_{60}O_{24}$ (1), $1{\cdot}2C_6H_4Br_2$ (1b), $1{\cdot}2C_6H_4F_2$ (1f), $1{\cdot}2C_6H_4Cl_2$ (1c)

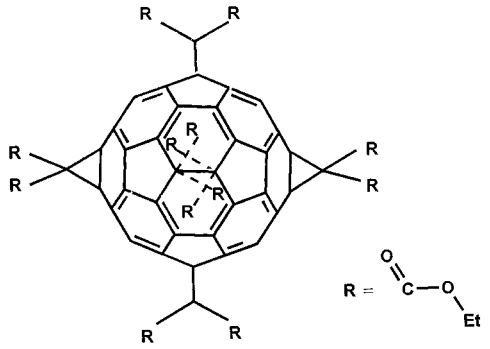

interesting bonding situation occurs in fullerenes and their derivatives that makes them particularly well suited for exploration of the above-mentioned correlations for a wide range of intermediate C−C bonds.

Experimental charge density studies on fullerenes are complicated on one hand by the generally poor quality of fullerene crystals and on the other hand by the high mobility of these molecules in the crystal lattice, which often manifests itself in static or dynamic disorder problems. Ordered structures are most likely to be obtained for substituted fullerenes and/or through cocrystallization with guest molecules. After several unsuccessful attempts to crystallize different C_{60}-fullerene derivatives we were able to grow suitable crystals of a highly substituted derivative, the T_h-symmetrical dodekakis(ethoxycarbonyl)-C_{60}-fullerene, $C_{102}H_{60}O_{24}$ (**1**),[22] which is known to cocrystallize with halogenobenzene solvents (Scheme 1). The crystal structure of (**1**) with 1,2-dibromobenzene as solvent (referred to as **1b**) was reported by Lamparth et al.[22] Since lighter atoms than bromine are better suited for a charge density study, attempts were made to crystallize the title compound from 1,2-difluoro- and 1,2-dichlorobenzene (**1f** and **1c**) and also from benzene. The latter experiments were unsuccessful, but proper quality crystals could be obtained for (**1f**) and (**1c**). For (**1c**) only a conventional room-temperature data set was measured, while for (**1f**) more than 350 000 reflections were collected at 100 K using synchrotron radiation. This data set was the subject of multipole refinement and the resulting model densities were analyzed quantitatively in terms of Bader's AIM theory.[10] An earlier experimental deformation density study on a C_{60}-derivative was reported by Irngartinger et al., where qualitative X−X deformation density maps were shown.[23]

Experimental Section

Yellow crystals were grown from a solution of the title compound (**1**) in 1,2-difluorobenzene (DFB) and 1,2-dichlorobenzene by very slow evaporation of the solvent. Room-temperature X-ray data for (**1c**) were measured on a conventional four circle diffractometer with Cu Kα radiation. The structure was solved and refined but not further considered for a charge density study.

X-ray diffraction data for (**1f**) were measured on a Huber four-circle diffractometer of the synchrotron beamline D3 of the storage ring DORIS III at the HASYLAB/DESY in Hamburg. A wavelength of 0.56 Å for the primary beam was used. The temperature was maintained at 100 K during the measurement with an Oxford Cryosystems N_2-gas stream cooling device. A Bruker 1 K CCD area detector allowed us to collect 365 235 reflections in 5 days up to a resolution of sin $\theta/\lambda = 1.26$ Å^{-1} (or $d = 0.40$ Å). The measurement strategy was planned with ASTRO[24] and had to be adjusted to the geometrical restrictions given by the Eulerian cradle of the diffractometer. Data were measured at four different positions of the detector. For the 2θ positions 30°, 0°, −30°, and −60° a total number of 12 028 frames were collected. The reflection profiles were found to be rather broad, probably due to the crystal mosaicity. Therefore a scan width of 0.3° in ω and θ was chosen. To obtain the low order reflections hidden by the beamstop, the detector−sample distance was increased from 4.0 to 6.5 cm for the $2\theta = 0°$ position and the beam stop adjusted accordingly. The exposure time ranged between 1 and 12 s. The data collection was monitored with SMART.[24] During integration with SAINT[24] the primary beam decay was corrected by using reference detector information. The standard narrow frame algorithm was used for integration. Unit cell parameters were obtained by a global unit cell refinement using 8192 reflections equally distributed over the 8 high order runs. No absorption correction was applied, the data were brought onto a common scale with the program SADABS.[24] Further details on the crystal data and the experimental conditions are given in Table 1.

TABLE 1: Crystal Data and Multipole Refinement for (1f)

empirical formula	$C_{102}H_{60}O_{24}{\cdot}2C_6H_4F_2$
molecular weight	1897.68
crystal system	triclinic
space group	$P\bar{1}$ (No. 2)
Z	1
temperature (K)	100
unit cell dimensions:	
a (Å)	13.1321(1)
b (Å)	13.6742(1)
c (Å)	14.7739(1)
α (deg)	97.30(2)
β (deg)	112.99(2)
γ (deg)	114.59(2)
V (Å^3)	2083.6(8)
calcd density (g·cm^{-3})	1.515
F(000)	980.0
abs coeff μ (mm^{-1})	0.07
crystal size (mm^3)	0.45 × 0.40 × 0.20
λ (Å)	0.5600
max. 2θ (deg)	89.61
$(\sin\theta/\lambda)_{max}$ (Å^{-1})	1.26
limiting indices	$-32 \le h \le 30$, $-34 \le k \le 33$, $-37 \le l \le 37$
number of collcd reflns	365235
symmetry ind reflns	65891
R_{int}	0.061

The structure was solved with SHELXS[25] and routine spherical atom refinements were carried out with SHELXL.[26] One fullerene molecule cocrystallizes with two difluorobenzene molecules. Since the center of the C_{60}-cage is on a crystallographic inversion center, the asymmetric unit consists of one-half of the substituted fullerene and one solvent molecule. The molecular structure is displayed in Figure 1a. One of the substituent's ethoxy groups was found to be disordered over two sites (Figure 1b). For these sites the refinement led to well-resolved atomic positions with a 1:2 ratio of the occupation factors. The positions of the hydrogen atoms could be located from difference Fourier maps, except for those of the disordered group, for which calculated positions were assigned and fixed.

Theoretical Calculations

Ab initio calculations were performed with the GAUSSIAN98[27] program package at the Hartree−Fock (HF) and density functional (B3LYP) levels of theory (cf. Table 2). The default

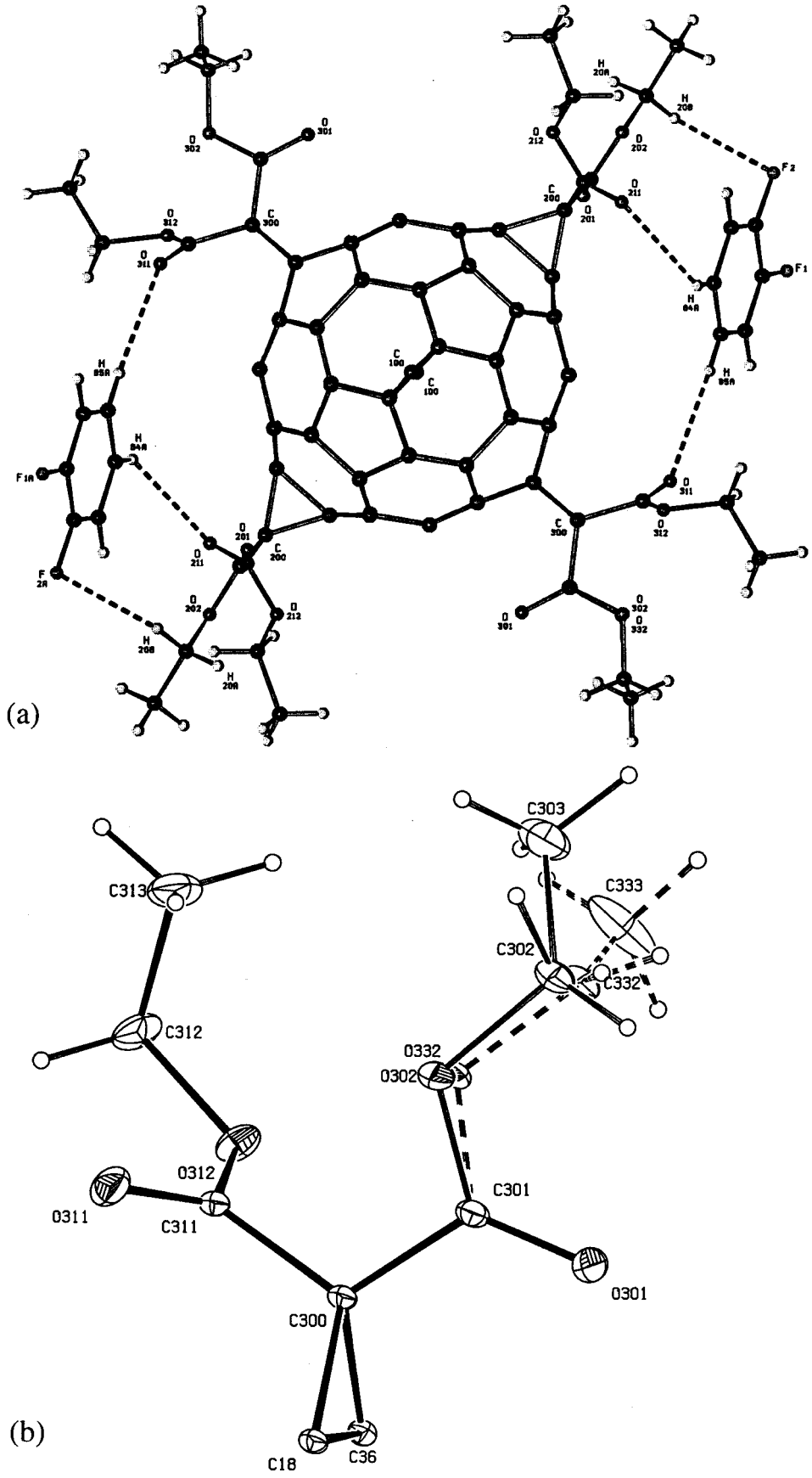

Figure 1. (a) Structure of the 1:2 complex of **1** with 1,2-difluorobenzene (SCHAKAL drawing).[42] The two substituents perpendicular to the paper plane are omitted for clarity. The complex is stabilized by three short host−guest contacts: C(84)−H(84)···O(211), H···O = 2.70(2) Å; C(85)−H(85)···O(311), H···O = 2.70(2) Å; C(202)−H(20b)···F(2), H···F = 2.60(2) Å. (b) ORTEP drawing[43] of the disordered substituent. U_{ij}'s at 50% probability.

TABLE 2: Summary of ab Initio Calculations

molecule	basis set	type
C_{60} (full I_h symmetry)	HF/3-21G	optimization
	HF/6−31 G**	optimization
	HF/6-311G**	optimization
dodekakis(ethoxycarbonyl)-C_{60} (**1**)	HF/3-21G*	single point (exp geom)
	HF/6-31G**	single point (exp geom)
	B3LYP/3-21G*	single point (exp geom)
	B3LYP/6-31G**	single point (exp geom)

options were used for SCF convergence and threshold limits applied for the final changes in the maximum forces and displacements (0.000 45 and 0.0018 au) in the geometry optimizations.

For (**1**), single point calculations with the experimental geometry were performed at the levels given in Table 2. Although various ab initio calculations for free C_{60} are known (see, for example, ref 28), even on post Hartree−Fock levels, we repeated a few HF calculations to generate reference topological data for a comparison with the substituted derivative (**1**). Because of the full icosahedral I_h symmetry of the C_{60} molecule, only the [6,5] and the [6,6] bond distances are to be optimized. All other parameters needed to describe the geometry of the molecule are fixed. This also holds for the two independent torsion angles describing the curvature of the molecule. These are τ_1 = [6,6]−[6,5]−[6,5] and τ_2 = [6,5]−[6,6]−[6,5], which satisfy tan $\tau_1 = \sqrt{5}-3$ and cos $\tau_2 = -1/3\sqrt{5}$.

Density Models and Multipole Refinement

The X-ray data were interpreted in terms of the Hansen-Coppens aspherical-atom formalism[12c] implemented into the XD program package.[29] The quantity $\sum_{\mathbf{H}} w_{\mathbf{H}} |F_{\mathrm{obs}}(\mathbf{H}) - kF_{\mathrm{calc}}(\mathbf{H})|^2$ was minimized using the statistical weight $w_{\mathbf{H}} = \sigma^{-2}(F_{\mathrm{obs}}(\mathbf{H}))$ and only those structure factors that met the criterion of $F_{\mathrm{obs}}(\mathbf{H}) \geq 3\sigma(F_{\mathrm{obs}}(\mathbf{H}))$ were included. The starting atomic parameters were based on a conventional refinement. The multipole expansion was truncated at the hexadecapolar level for the heavy atoms, while the deformation of the hydrogen atoms was described by bond-directed dipoles. The core and the spherical valence densities were composed of HF wave functions expanded over Slater type basis functions.[30] For the deformation terms single-ζ orbitals with fixed, energy-optimized Slater exponents were used.[30] No charge transfer between the fullerene derivative and the difluorobenzene molecule was allowed, and the unit cell was kept neutral during the refinement. The C−H and O−H distances were kept constant (1.09 and 0.95 Å, respectively). To reduce the number of variables, constraints based on chemical and site symmetries were imposed. These restrictions can be best explored with reference to the symmetry of the unsubstituted cage. In the I_h isomer of the C_{60} molecule all C-atoms are equivalent, each occupying a site of C_s local symmetry. Based on the Kekulé structure, two different types of bonds (D[6,6] double and S[6,5] single) can be distinguished. Due to the substituents in the title compound, 6 out of the 30 formally double bonds present in C_{60} become single bonds and the 60 equivalent single bonds split into 3 sets. This reduction of symmetry is depicted in Scheme 2. There are 3 chemically different C-atoms. A type C1 atom is involved in 3 single bonds; 1 long one (S1[6,6]), that is part of the cyclopropane ring attached at the 1,6 position and 2 equivalent but shorter ones (S2[6,5]). A type C2 atom forms a double bond with type C3 (D1[6,6]) and 2 different single bonds (S2[6,5] and S3[6,5]). Finally, the bonds to atoms of type **C3** are D1[6,6], S3[6,5], and S4[6,5]. Since the molecular symmetry in the crystal is C_i, the 30 crystallographically unique cage carbon atoms fall into 6 C1, 12 C2, and 12 C3 chemical types and form 12 D1, 3 S1, 12 S2, 12 S3, and 6 S4 type bonds. Among the different C atom types only type C1 has a local C_s symmetry that was maintained during the refinement. In the substituents there are 6 exocyclic S5 bonds (in the 3 cyclopropane rings), 6 C−CO(OEt), and 6 single C−C bonds in the ethyl groups. Grouping of the C−C bonds this way is justified by the distribution of bond distances. As discussed below, the distances within each group are statistically equal, but they are significantly different for different chemical types.

SCHEME 2: Atomic and Bonding Equivalence in Free C_{60} (A) and in the Hexakis Adduct (1) (B)

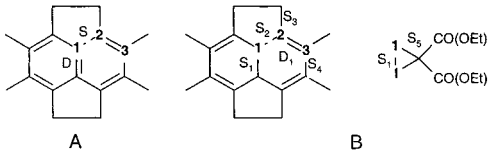

A B

As already mentioned, an ethoxy group of one ethoxycarbonyl substituent was found to be disordered, but this disorder could be well resolved with a ratio of one-to-two for the occupation factors of the corresponding atoms. A preliminary multipole refinement, in the course of which, all but the disordered sites were described by the aspherical-atom model, led to the same ratio. In the final multipole model this ratio was fixed and chemical constraints were applied to all equivalent atoms of the substituents. On the deformation density of the methyl and the exo-cyclopropane C-atoms, respectively, C_{3v} and C_{2v} site symmetries were imposed. Restrictions among the multipole populations of the C-atoms in 1,2-difluorobenzene (DFB) were also introduced to mimic the symmetry expected for the isolated molecule. Thus, the 2 fluoro-substituted C-atoms were considered to be equivalent and so were the 2 F-atoms, as well as the 4 remaining ring C-atoms. For the latter type C_s site symmetries were invoked, while the deformation density of the F-atoms was described by bond directed multipoles ($m = 0$ for all l) exhibiting rotational symmetry along the bonds. The H-atoms attached to equivalent atoms were kept the same. Further constraints were introduced among the atomic displacement parameters. All C−C bonds were kept "rigid" in the sense of Hirshfeld's rigid-bond postulate.[31] This was achieved by starting with the anisotropic displacement amplitudes, predicted by the rigid-body model,[32] and by constraining their shifts according to the rigid-bond condition. Individual isotropic displacement parameters for each H-atom were refined independently, but those assigned to the disorder sites were constrained to the values of the corresponding nondisorder sites. The results of three refinements, differing in the treatment of the radial exponents of the deformation density, are discussed in the following section. The rigid-bond restrictions allowed us to reach a convergence with the κ' parameters included as variables in the full-matrix least-squares refinement. We call this approach the κ'-unrestricted multipole model (KUMM), in conjuction with the corresponding restricted model (KRMM). The refinement in which energy-optimized exponents were kept fixed ($\kappa' = 1$) is referred to as K1MM. Details of the different refinements and the final figures of merit are summarized in Table 3, and κ and κ' values obtained after the KUMM and KRMM refinements are in Table 4.

Results and Discussion

(a) Crystal and Molecular Structure. Figure 1 shows the 1:2 complex of (**1**) and DFB in the crystal structure. The

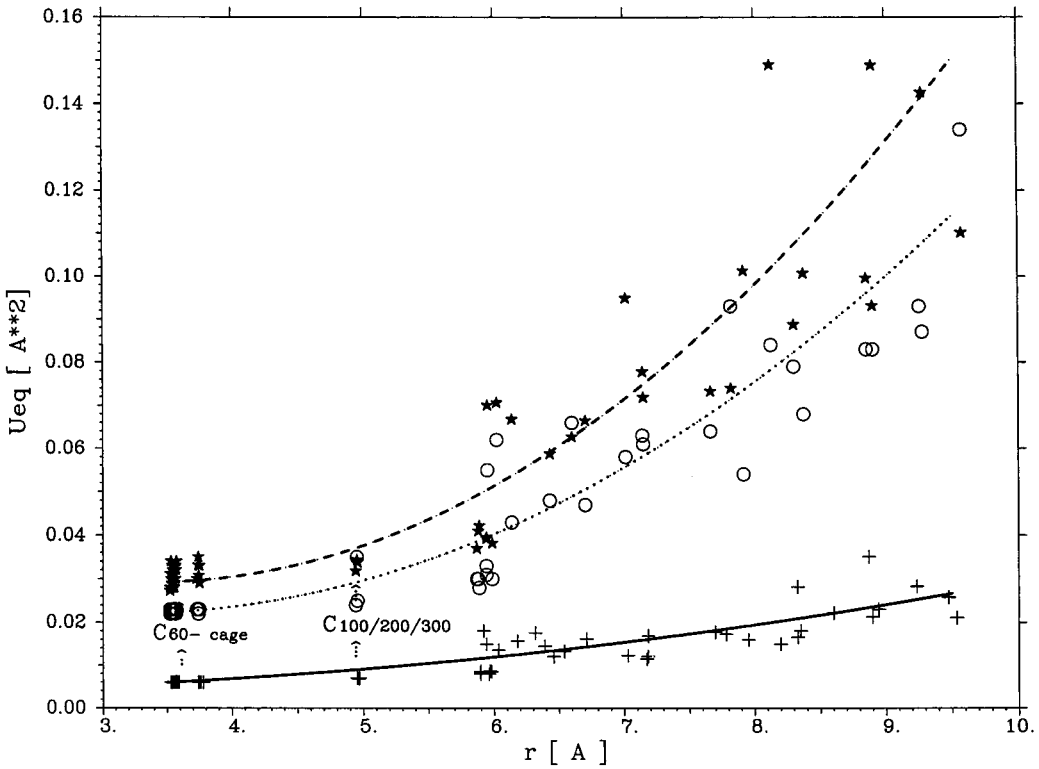

Figure 2. Equivalent isotropic displacement parameters U_{eq} plotted versus atomic distances r (Å) from the C_{60}-cage center for **1b** (circles, dotted line) and **1c** (stars, dashed line) at room temperature and for **1f** (crosses, solid line) at 100 K.

TABLE 3: Figure of Merits of Different Multipole Refinement[a]

	K1MM	KRMM	KUMM
NREF			
($\|F_o\| > 3\sigma(\|F_o\|$)		35615	
NVAR	1099	1099	1112
NCON		216	
NV	883	883	896
R_w	0.0274	0.0274	0.0268
GOF	2.90	2.86	2.80

[a] There were NCON number of constraints applied among NVAR original variables leading to NV free variables.

TABLE 4: Summary of κ and κ' Values for Chemically Independent Atoms (Atom Numbering in Scheme 2b and Figure 1b)

	κ(KUMM)	κ'(KUMM)	κ(KRMM)	κ'(KRMM)
		Cage		
C(1)	1.002(3)	0.91(2)	1.005(3)	0.87
C(2)	1.013(3)	0.98(2)	1.014(3)	0.87
C(3)	1.001(3)	0.85(1)	1.014(3)	0.87
		Substituent		
C(100)	1.008(2)	0.80(2)	1.021(5)	0.87
C(101)	0.990(3)	0.88(1)	1.010(3)	0.88
C(102)	0.949(3)	0.816(8)	0.974(5)	0.95
C(103)	0.947(3)	0.87(3)	0.961(5)	0.97

mobility of the C_{60} molecule in the crystal at 100 K and at room-temperature is compared in Figure 2, where the equivalent isotropic displacement parameters (U_{eq} values) of all atoms are plotted versus their distances from the cage center. For the two room-temperature structures (**1b**) and (**1f**) the U_{eq} values increase almost exponentially with this distance, while for the 100 K structure (**1f**) the dependence is linear with a rather flat slope. The lowest U_{eq}'s are seen for the atoms on the cage surfaces, ranging from 0.02 to 0.035 Å^2 for the room-temperature data and are close to 0.005 Å^2 for (**1f**), indicating a significant reduction of thermal motion at 100 K also for the cage atoms.

The average bond distances of the five chemically different bonds of the C_{60} cage are listed in Table 5. The deformation of the fullerene cage due to the [1+2] cycloaddition is most clearly indicated by the lengthening of the S1[6,6] bond between the bridging carbon atoms to 1.595(4) Å in (**1f**). Similar values have been published earlier.[33−35] The D1[6,6] bond is only slightly affected, the average value of 1.397(3) Å is close to those found for monosubstituted C_{60} derivatives (∼1.38 Å),[33] and by electron diffraction for the free C_{60} (1.40 Å),[36] but somewhat longer than the theoretical value of 1.371 Å obtained from the HF/6-311G** geometry optimization (cf. Table 6).

Two of the three [6,5] bonds (S2 and S4) are longer, while S3 is shorter than those found for the monosubstituted (1.45 Å)[33] or free C_{60} (1.458(6) Å).[36] The lengthening of the bridging [6,6] bond is accompanied by an outward displacement of the bridging atoms from the molecular surface. The average distance of the nonbridging atoms from the cage center (R = 3.55(2) Å) is close to the value (R = 3.53(3) Å) found for the monosubstituted C_{60} sphere and to the result of our theoretical calculation (R = 3.53 Å). The average distance of the bridging atoms from the center is R = 3.75(2) Å. This is also in accord with previous findings for monosubstituted derivatives; i.e., these atoms are situated approximately 0.2 Å away from the surface of the cage.[33,37]

The DFB molecules are located between two substituents. The hexaadduct/solvent interaction is stabilized by three C−H···O/C−H···F contacts (see Figure 1a).

(b) Charge Density and Bond Topological Properties. Based on X−X deformation density maps, Irngartinger et al.[23] found that deformation density maxima were outwardly shifted from the surface of the cage. This observation can be confirmed by the inspection of theoretical deformation density maps of free C_{60} and an experimental static map of (**1f**). In Figure 3 such maps, calculated in comparable planes through cage equators, are displayed. Significant nonzero deformation density

TABLE 5: Averaged Bond Lengths for (1f) (Å), Electron Density ρ (e Å^{-3}), and the Laplacian $\nabla^2\rho$ and λ_3 (e Å^{-5}) at the Bond Critical Points

			K1MM			KRMM			KUMM			HF/6-31G**			B3LYP/6-31G**		
type	length	no.	ρ	$\nabla^2\rho$	λ_3	ρ	$\nabla^2\rho$	λ_3	ρ	$\nabla^2\rho$	λ_3	ρ	$\nabla^2\rho$	λ_3	ρ	$\nabla^2\rho$	λ_3
S5	1.520(5)	6	1.58(1)	−6.1(2)	12.6(1)	1.56(1)	−6.0(2)	11.7(1)	1.56(1)	−6.2(2)	11.3(1)	1.62(1)	−12.2(2)	7.0(1)	1.57(1)	−9.9(2)	8.2(1)
S1 [6,6]	1.595(4)	3	1.35(1)	−2.0(2)	12.0(1)	1.32(1)	−1.3(2)	11.7(1)	1.33(1)	−1.8(2)	11.6(1)	1.40(1)	−7.7(2)	6.8(1)	1.35(1)	−5.7(2)	7.9(1)
S2 [6,5]	1.495(3)	12	1.80(2)	−12.8(3)	12.5(1)	1.76(2)	−12.1(3)	11.3(1)	1.78(2)	−12.4(3)	11.9(1)	1.83(1)	−17.6(3)	7.3(1)	1.76(1)	−14.6(2)	8.7(1)
S4 [6,5]	1.475(2)	6	1.85(1)	−12.7(1)	13.1(1)	1.82(1)	−12.7(1)	11.5(1)	1.84(1)	−13.4(1)	10.9(1)	1.88(1)	−18.6(2)	7.3(1)	1.81(1)	−15.5(2)	8.6(1)
S3 [6,5]	1.434(2)	12	2.01(1)	−15.8(2)	12.9(1)	1.96(1)	−15.0(2)	11.4(1)	1.99(1)	−15.2(2)	11.6(1)	2.03(1)	−20.7(2)	7.2(1)	1.97(1)	−17.7(2)	8.6(1)
D1 [6,6]	1.397(3)	12	2.18(1)	−19.1(3)	12.7(1)	2.13(1)	−18.5(3)	10.8(1)	2.15(1)	−18.9(3)	11.1(1)	2.15(1)	−22.5(3)	6.7(1)	2.09(1)	−19.7(3)	8.2(1)

TABLE 6: Critical Points in Free C_{60} from HF/6-311G**

type[a]	distance (Å) bond path (Å)	ρ (e Å^{-3})	$\nabla^2\rho$ (e Å^{-5})	ϵ
D[6,6] bond (3,−1)	1.371 1.372	2.232	−25.137	0.29
S[6,5] bond (3,−1)	1.448 1.450	1.966	−20.476	0.16
6 memb ring (3,1)		0.146	3.858	
5 memb ring (3,1)		0.299	7.040	
cage (3,3)		0.00006	0.0025	

[a] The integer pair (3,−1) indicates a bond critical point, (3,1) is for a ring, and (3,3) is for a cage critical point.

is concentrated in a shell of ∼1.9 Å broadness around the cage surface with the subshell outside the sphere being 0.3−0.4 Å broader than the inner one. This effect is even more visible, when maps calculated in planes below and above the cage's surface (by 0.4 Å) are compared (Figure 4). For both the five- and six-membered rings, higher density is found above than below the plane of the rings. On the other hand, the bond path lengths for the bonds in question are only slightly longer than the bond distances (0.001−0.002 Å). This is in accord with the results obtained for the bent bonds of the cyclopropane ring in bullvalene.[13]

Topological descriptors were derived from a HF/6-311G** optimization of the free C_{60} to serve as reference and to compare with the experimental and theoretical findings of the hexaadduct (Table 6). From the charge density values at the bond critical points, $\rho_{66} = 2.232$ and $\rho_{56} = 1.966$ e Å^{-3} bond orders of $n \approx 1.83$ and $n \approx 1.38$ can be estimated.[13,20a] In addition to the bond critical points, Table 6 lists also ring (RCP) and a cage critical point (CCP), the latter in the geometric center of the C_{60} sphere with almost zero electron density.

The experimental static ED's, corresponding to the three multipole models, were analyzed with the aid of XDPROP, the property program of the XD package (see Table 5). All intramolecular critical points in the asymmetric unit were located and for each model the associated properties ($P = \rho(\mathbf{r}_{BCP})$, λ_1, λ_2, λ_3, and $\nabla^2\rho(\mathbf{r}_{BCP})$) are compared here with those obtained by the topological analysis of theoretical densities (performed by the AIMPAC program system[38]). This evaluation involves 89 BCP (45 for the C_{60}, 36 for the ethoxycarbonyl groups, and 8 for DFB), 20 RCP (6 five-membered, 10 six-membered rings in C_{60}, 3 three-membered rings in the ethoxycarbonyl groups, and 1 six-membered in DFB), and 1 CCP properties. In the following, we concentrate on the S1−S5 and D1 type C−C bonds. The theoretical properties considered in detail are those obtained at the HF and B3LYP levels (referred to as HF and DFT, respectively), both utilizing the 6-31G** basis set. An obvious reason for using B3LYP/6-31G** properties as references is that the radial exponents of the KRMM have been optimized to densities calculated at this level.

Figure 5 displays $\rho(\mathbf{r}_{BCP})$ vs bond-distance relationships. The straight lines fitted to different theoretical $\rho(\mathbf{r}_{BCP})$ values (Figure 5a) have practically identical slopes but the bond density increases going from the HF/3-21G* via B3LYP/6-31G** to the HF/6-31G** level. The lines corresponding to the three model densities (Figure 5b) exhibit a high level of internal consistency; that is, the data points resulting from different refinements are statistically equal. The experimental values scatter in a narrow range around the theoretical lines of the higher basis set. The assumption of a linear relationship is statistically confirmed, though data points corresponding to the S5 type bonds appear to be outliers. On the basis of the fits obtained for the model densities, $\rho(\mathbf{r}_{BCP})$ values of various C−C bonds can be predicted.

Table 7 compares the interpolated X-ray density data with those obtained by independent experimental studies for the C−C bonds in diamond and in different hydrocarbons. The KUMM appears to predict this topological index slightly better than either the K1MM or KRMM.

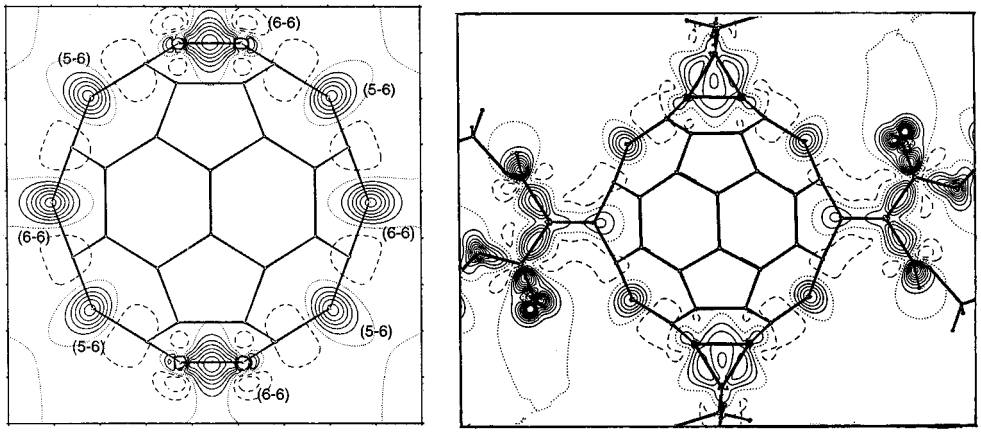

Figure 3. (Left) theoretical deformation density of nonsubstituted C_{60} from HF/6-311G** optimization. Right: Static deformation density map of **1f** after multipole refinement (KRMM model). In both cases an equatorial plane through two opposite 6−6 bonds is displayed (the plane contains two 6−6 bonds and cuts four 5−6 and two 6−6 bonds, as indicated on the left).

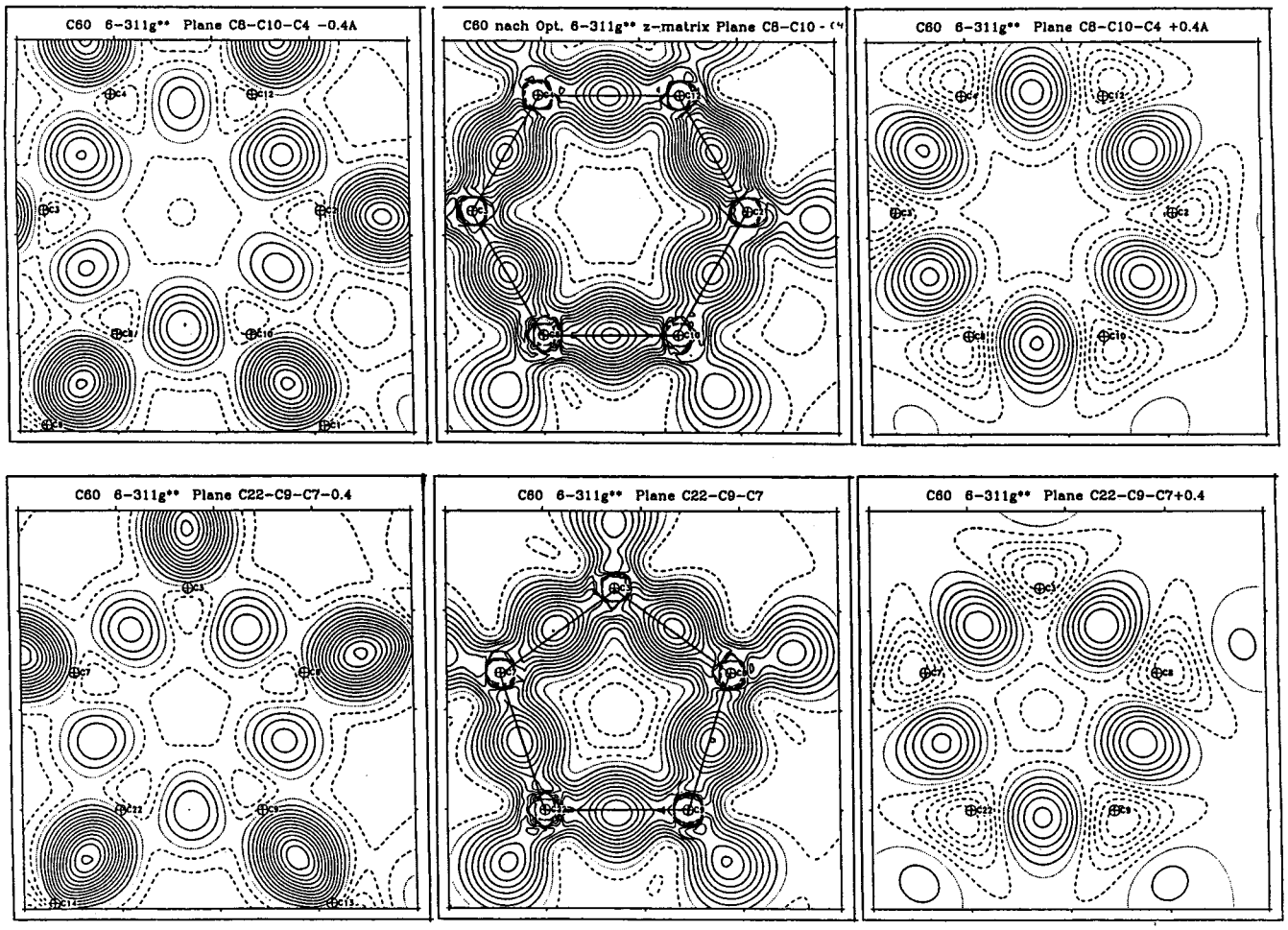

Figure 4. Theoretical deformation densities of nonsubstituted C_{60} from HF/6-311G** optimization. Above: plane through a six-membered ring (center) and planes 0.4 Å below and 0.4 Å above the central plane (left and right, respectively) (below/above are defined as directed inward/outward from the C_{60} sphere). Below: corresponding planes for a five-membered ring.

TABLE 7: $\rho(\mathbf{r}_{BCP})$ for Various C−C Bonds As Derived from X-ray Densities and by Interpolations of the Results from the Study of the Title Compound[a]

	R (Å)	$\rho(\mathbf{r}_{BCP})_{exp}$ (e Å^{-3})	$\rho(\mathbf{r}_{BCP})_{K1MM}$ (e Å^{-3})	$\rho(\mathbf{r}_{BCP})_{KUMM}$ (e Å^{-3})	$\rho(\mathbf{r}_{BCP})_{KRMM}$ (e Å^{-3})
diamond[b]	1.5445	1.596	1.549	1.521	1.530
ethane[c]	1.510	1.61	1.70	1.66	1.68
ethylene[c]	1.336	2.16	2.44	2.38	2.41
acetylene[c]	1.183	2.84	3.04	3.00	3.06
benzene[d]	1.392	2.15	2.20	2.15	2.18
bulvallene[e]					
$C(sp^3)-C(sp^2)$	1.5157	1.78	1.67	1.64	1.65
$C(sp^2)-C(sp^2)$	1.3450	2.36	2.40	2.34	2.37
$C(sp^2)-C(r)$	1.4727	1.92	1.86	1.82	1.83
C(r)−C(r)	1.5353	1.54	1.59	1.56	1.57

[a] The parameters of the linear fit $\rho(\mathbf{r}_{BCP}) = aR + b$ are $a = -4.260$, $b = 8.129$ (K1MM); $a = -4.100$, $b = 7.853$ (KUMM); and $a = -4.233$, $b = 8.068$ (KRMM). [b] Reference 39. [c] Reference 40. [d] Reference 41. [e] Reference 13.

Table 5 lists BCP properties of all bond types obtained from wave functions and from X-ray data by the three refinement models. The entries represent arithmetic mean values obtained by averaging each property over the bonds within each bond type (the standard deviation is evaluated with respect to the sample mean). All topological indices but λ_3 exhibit a monotone decrease in absolute value as the bond distance increases. No systematic trend can be established for the change in the parallel curvature as a function of the interatomic separation. The HF values of all properties but $\rho(\mathbf{r}_{BCP})$ are somewhat lower than those given by the DFT. The density and the parallel curvatures obtained by the κ'-models (KRMM and KUMM) are lower, while all other indices are higher than the corresponding values associated with K1MM. To explore the reproducibility of the experimental method and the performance of different models in accounting for theoretical results, we calculated R-factor type agreement indices for each BCP property ($R = \sum_{bond}(P_{method1} - P_{method2})^2/\sum_{bond}P_{method2}^2$). Table 8 shows, for example, that the average relative discrepancy between the two theoretical $\rho(\mathbf{r}_{BCP})$ values (R[DFT-HF]) amounts to 3.2%, which is of the same magnitude as the KRMM-HF deviation but larger than any other discrepancy obtained for this property. Theoretical deviations in the perpendicular curvatures are close in value to those found between theory and experiment (R[K1MM-DFT], R[KRMM-HF], and R[KUMM-HF]), as well as to those found

TABLE 8: Agreement Indices between BCP Properties by Different Methods

method 1	method 2	ρ	λ_1	λ_2	λ_3	$\nabla^2\rho$
DFT	HF/6-31G**	3.2	6.2	5.6	18.8	15.7
K1MM		1.9	3.6	7.7	66.9	35.5
KRMM		3.4	6.8	5.8	34.5	44.2
KUMM		2.7	6.0	5.9	38.2	42.8
K1MM	B3LYP/6-31G**	2.7	8.9	10.9	51.1	18.4
KRMM		1.2	2.2	5.1	36.6	21.1
KUMM		1.9	3.4	6.1	36.5	18.7
KRMM	K1MM	2.1	8.3	6.3	10.7	4.5
KUMM		1.1	6.4	5.3	11.0	3.2
KUMM	KRMM	1.1	2.3	2.3	3.7	3.3

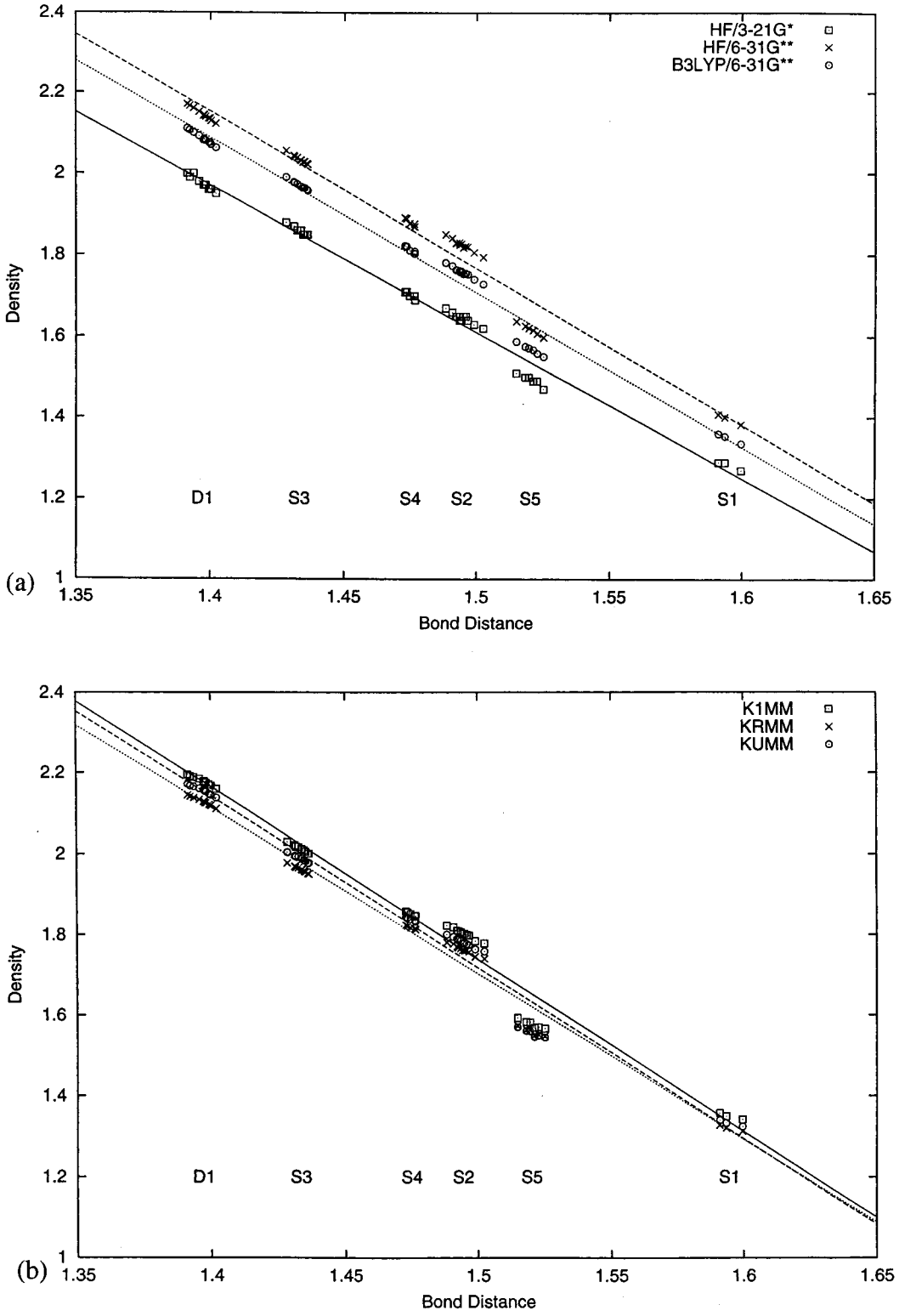

Figure 5. Variation of $\rho(\mathbf{r}_{BCP})$ vs bond distance. Data points are fitted by straight lines. (a) Theoretical results, least squares lines for HF/3-21G* solid, for B3LYP/6-31G** dotted, for HF/6-31G** dashed. (b) Experimental results, left side, lines for K1MM solid, for KRMM dotted, and for KUMM dashed. Units are e $Å^{-3}$ and Å. The definition of bond types D1 and S1−S5 is given in Scheme 2b.

by comparing κ'-refined and constrained models (R[KRMM-K1MM] and R[KUMM-K1MM]). It is a general observation that κ'-refined properties are in a better agreement with the DFT than with the HF results and show the best model vs model correlation. This is true even for λ_3, the least well reproduced property of them all. In terms of the Laplacian, on the other hand, K1MM seems to agree slightly better with both theories.

Conclusion

This state-of-the art study confirms that presently available technical standards allow for accurate experimental charge density determinations on structures containing more than 100 atoms. The combination of synchrotron primary radiation and CCD area detection can lead to precise, high resolution data

within a reasonable measurement time. Uncertainties in experimental properties are subject not only to the errors but also to the interpretation of the measurements. With improving data quality, model ambiguities remain the main source of uncertainties. Commonly used statistical descriptors (figures of merit of the fit, significance tests and standard deviations of parameter estimates) are either difficult to evaluate (for all possible selections of free variables) or fail to filter out the ambiguities in question. The problem of reliability is thus often explored by comparing the results with those obtained from quantum chemical calculations or with those derived from independent measurements for chemically related systems.

In this study we compared experimental BCP properties of different C−C bonds in a substituted C_{60} derivative, obtained by three multipole models, to each other and to those derived by theoretical methods at HF/6-31G** and B3LYP/6-31G** levels at the experimental geometry. These calculations have been adopted as benchmarks and affordable limits for larger molecules in numerous model studies, as well as in combined studies aiming at comparison of experimental and theoretical BCP properties.[18,19] Since there are six different C−C bond types in the title compound, each one occurring with at least a 3-fold redundancy, a statistical analysis of the BCP properties is justified. The reproducibility of the experimental method was monitored in terms of relative deviations between experimental and theoretical properties and properties derived by models of different flexibility (constrained and unconstrained κ'-refinements). These simple quantities, averaged over all bonds, appear to be suitable indicators of reproducibility and overall accuracy. The results support earlier observations that among the bond topological indices $\rho(\mathbf{r}_{BCP})/\lambda_3$ is the most/least reproducible. The frequently cited value of 0.05 e/Å^3 for the error, associated with X-ray charge densities, cannot simply be adopted as a standard figure, if the analysis relies on high resolution and highly redundant data. In this case, at least for C−C bonds, the uncertainty in $\rho(\mathbf{r}_{BCP})$ estimates can be reduced below the quoted value. The results clearly demonstrate that consideration of the expansion−contraction of the deformation radial functions is essential if meaningful comparison between theoretical and experimental curvatures is to be made. This is less obvious when the comparison is based on the Laplacian. Bias in the principal curvatures of the experimental density caused by model inadequacies/ambiguities can cancel each other, leading to $\nabla^2\rho(\mathbf{r}_{BCP})$ values in apparent agreement with theory. The refinement of the associated parameters (κ') against X-ray data is often troublesome. Because of their strong correlation with other variables, especially with ADP's and monopole populations, their refinement fails in most cases. If a block-diagonal approach is enforced, their correlation with other variables cannot be evaluated. Imposing rigid-bond conditions seems to overcome the problem in an elegant and easy-to-handle way. The method, at least for C−C bonds, led to stable convergence and to reasonable estimates in overall satisfactory agreement with theory. It has also been shown that such restriction successfully reduced the bias in the Laplacian along the bond path of highly polarized carbonyl bonds.[19] The KRMM seems to be the model of preference if κ' refinement fails or the data quality does not allow for it, but it seems to bias experimental properties toward DFT properties.

Acknowledgment. Funds were gratefully accepted from the Bundesminister für Forschung und Technologie (BMBF, grant 05 SM8KEA0), from the Deutsche Forschungsgemeinschaft, grant LU 222/21-1, and the Fonds der Chemischen Industrie. We thank Professor A. Hirsch (Erlangen/Germany) for the sample of the fullerene derivative (**1**).

References and Notes

(1) Koritsanszky, T.; Flaig, R.; Zobel, D.; Krane, H.-G.; Morgenroth, W.; Luger, P. *Science* **1998**, *279*, 356.

(2) Iversen, B. B.; Larsen, F. K.; Pinkerton, A. A.; Martin, A.; Darovsky, A.; Reynolds, P. A. *Acta Crystallogr.* **1999**, *B55*, 363.

(3) Graafsma, H.; Svensson, S. O.; Kvick A. *J. Appl. Crystallogr.* **1997**, *30*, 957.

(4) Mallinson, P. R.; Barr, G.; Coles, S. J.; Guru Row: T. N.; MacNicol, D. D.; Teat, S. J.; Wozniak, K. J. *Synchrotron Rad.* **2000**, *7*, 160.

(5) Flaig, R.; Koritsanszky, T.; Janczak, J.; Krane, H.-G.; Morgenroth, W.; Luger, P. *Angew. Chem., Int. Ed. Engl.* **1999**, *38*, 1397.

(6) Jelsch, C.; Pichon-Pesme, V.; Lecomte, C.; Aubry A. *Acta Crystallogr.* **1998**, *D54*, 1306.

(7) Housset, D.; Benabicha, F.; Pichon-Pesme, V.; Jelsch, C.; Maierhofer, A.; David, S.; Fontecilla-Camps, J. C.; Lecomte, C. *Acta Crystallogr.* **2000**, *D56*, 151.

(8) Jelsch, C.; Teeter, M. M.; Lamzin, V.; Pichon-Pesme, V.; Blessing, R. H.; Lecomte, C. *Proc. Natl. Acad. Sci. U.S.A.* **2000**, *97*, 3171.

(9) (a) Hohenberg, P.; Kohn, W. *Phys. Rev.* **1964**, 136, B864. (b) Kohn, W.; Sham, L. J. *Phys. Rev.* **1965**, *140*, A1133.

(10) Bader, R. F. W. *Atoms in Molecules—A Quantum Theory*; Oxford University Press: Oxford, U.K., 1990.

(11) Koritsanszky, T.; Coppens, P. *Chem. Rev.* **2001**, *101*, 1583.

(12) (a) Hirschfeld, F. L. *Acta Crystallogr.* **1971**, *B27*, 769. (b) Stewart, R. F. *Acta Crystallogr.* **1976**, *A32*, 565. (c) Hansen, N. K.; Coppens, P. *Acta Crystallogr.* **1978**, *A34*, 909.

(13) Koritsanszky, T.; Buschmann, J.; Luger, P. *J. Phys. Chem.* **1996**, *100*, 10547.

(14) Gatti, C.; Bianchi, R.; Destro, R.; Merati, F. *J. Mol. Struct. (THEOCHEM)* **1992**, *255*, 409.

(15) Bianchi, R.; Gatti, C.; Adovasio, V.; Nardelli, M. *Acta Crystallogr.* **1996**, *B52*, 471.

(16) Volkov, A.; Abramov, Yu.; Coppens, P.; Gatti, C. *Acta Crystallogr.* **2000**, *A56*, 332.

(17) Stewart, R. F.; Davidson, E.R.; Simpson, W. T. *J. Chem. Phys.* **1965**, *42*, 3175.

(18) Abramov, Yu.; Volkov, A.; Coppens, P. *Chem. Phys. Lett.* **1999**, *311*, 81.

(19) Volkov, A.; Abramov, Yu.; Coppens, P. *Acta Crystallogr.* **2001**, *A57*, 272.

(20) (a) Bader, R. F. W.; Slee, T. S.; Cremer, D.; Kraka, E. *J. Am. Chem. Soc.* **1983**, *105*, 5061. (b) Wiberg, K. B.; Bader R. F. W.; Lau, C. D. H. *J. Am. Chem. Soc.* **1987**, *109*, 985. (c) Cremer, D.; Kraka, E.; Slee, T. S.; Bader, R. F. W.; Lau, C. D. H.; Nguyen-Dang, T. T.; MacDougall, P. J. *J. Am. Chem. Soc.* **1983**, *105*, 5069. (d) Alkorta, I.; Barrios, L.; Rozas, I.; Elguero, J. *J. Mol. Struct. (THEOCHEM)* **2000**, *496*, 131.

(21) (a) Flensburg, C.; Larsen, S.; Stewart, R. F. *J. Phys. Chem.* **1995**, *99*, 10130. (b) Roversi, P.; Barzaghi, M.; Merati, F.; Destro, R. *Can. J. Chem.* **1996**, *74*, 1145. (c) Mallinson, P. R.; Wozniak, K.; Smith, G. T.; McCormack, K. L.; Yufit, D. S. *J. Am. Chem. Soc.* **1997**, *119*, 11502.

(22) (a) Lamparth, I.; Maichle-Mössmer, C.; Hirsch, A. *Angew. Chem.* **1995**, *107*, 1755. (b) Bühl, M.; Hirsch, A. *Chem. Rev.* **2001**, *101*, 1153.

(23) Irngartinger, H.; Weber, A.; Oeser, T. *Angew. Chem.* **1999**, *111*, 1356.

(24) (a) Bruker **1996**. ASTRO, SMART and SAINT-Plus. Data Collection and Processing Software for the SMART System. Bruker-AXS Inc., Madison, WI. (b) Blessing, R. H. *Acta Crystallogr.* **1995**, *A51*, 33.

(25) Sheldrick, G. M.; Krüger, C.; Goddard, R. *Crystallographic Computing 3*; Oxford University Press: Oxford, U.K., 1987; p 175.

(26) Sheldrick, G. M. **1997**. SHELXL-97, A Program for Refinement of Structures. Universität Göttingen.

(27) Frisch, M. J.; Trucks, G. W.; Schlegel, H. B.; Scuseria, G. E.; Robb, M. A.; Cheeseman, J. R.; Zakrzewski, V. G.; Montgomery, J. A., Jr.; Stratmann, R. E.; Burant, J. C.; Dapprich, S.; Millam, J. M.; Daniels, A. D.; Kudin, K. N.; Strain, M. C.; Farkas, O.; Tomasi, J.; Barone, V.; Cossi, M.; Cammi, R.; Mennucci, B.; Pomelli, C.; Adamo, C.; Clifford, S.; Ochterski, J.; Petersson, G. A.; Ayala, P. Y.; Cui, Q.; Morokuma, K.; Malick, D. K.; Rabuck, A. D.; Raghavachari, K.; Foresman, J. B.; Cioslowski, J.; Ortiz, J. V.; Stefanov, B. B.; Liu, G.; Liashenko, A.; Piskorz, P.; Komaromi, I.; Gomperts, R.; Martin, R. L.; Fox, D. J.; Keith, T.; Al-Laam, M. A.; Peng, C.Y.; Nanayakkara, A.; Gonzalez, C.; Challacombe, M.; Gill, P. M. W.; Johnson, B.; Chen, W.; Wong, M. W.; Andres, J. L.; Gonzalez, C.; Head-Gordon, M.; Replogle, E. S.; Pople, J. A. *Gaussian 98*, Revision A.6; Gaussian, Inc.: Pittsburgh, PA, 1998.

(28) Häser, M.; Almhöf, J.; Scuseria, G. E. *Chem. Phys. Lett.* **1991**, *181*, 497.

(29) Koritsanszky, T.; Howard, S.; Mallinson, P. R.; Su, Z. W.; Richter, T.; Hansen, N. K. XD, A Computer Program Package for Multipole Refinement and Analysis of Charge Densities from X-ray Diffraction Data, *User's Manual*; Freie Universität Berlin: Berlin, 1995.

(30) Clementi, E.; Roetti, C. *At. Data Nucl. Data Tables* **1974** *14*, 177.

(31) Hirshfeld, F. L. *Acta Crystallogr.* **1976**, *A32*, 239.

(32) Schomaker, V.; Trueblood, K. N. *Acta Crystallogr.* **1968**, *B24*, 63.

(33) Ramm, M.; Luger, P.; Strümpel, M.; Beurskens, G.; Averdung, J.; Mattay, J. *Z. Kristallogr.* **1998**, *213*, 69.

(34) Tezuka, Y.; Kawasaki, N.; Yajima, H.; Ishii, T.; Oyama, T.; Takeuchi, K.; Nakao, A.; Takayama, C. *Acta Crystallogr.* **1996**, *C52*, 1008.

(35) Paulus, E. F.; Bingel, C. *Acta Crystallogr.* **1995**, *C51*, 141.

(36) Hedberg, K.; Hedberg, L.; Bethune, D. S.; Brown, C. A.; Dorn, H. C.; Johnson, R. D.; de Vries, M. *Science* **1991**, *254*, 410.

(37) Zobel, D.; Strümpel, M.; Luger, P.; Ramm, M.; Duczek, W.; Niclas, H.-J. *Z. Kristallogr.* **1999**, *214*, 413.

(38) Cheeseman, J.; Keith, T. A.; Bader, R. F. W. AIMPAC program package; McMaster University: Hamilton, Ontario, 1992.

(39) Abramov, Yu. A.; Okamura, F. P. *Acta Crystallogr.* **1997**, *A53*, 187.

(40) Kapphahn, M.; Tsirelson, V. G.; Ozerov, R. P. *Port. Phys.* **1988**, *19*, 213.

(41) Stewart, R. F. In *Applications of Charge Density Research to Chemistry and Drug Design*; Jeffrey, G. A.; Piniella, J. F., Eds.; Plenum Press: New York, 1991.

(42) Keller, E. SCHAKAL88. A Fortran Program for the Graphical Representation of Molecular and Crystallographic Models; University Freiburg: Freiburg, Germany, 1988.

(43) Johnson, C. K. ORTEP II, Report ORNL-5138; Oak Ridge National Laboratory: Oak Ridge, TN, 1976.